Measurement of DNA-Dependent Protein Kinase Phosphorylation Using Flow Cytometry Provides a Reliable Estimate of DNA Repair Capacity

Authors: Abramenkovs, Andris, and Stenerlöw, Bo

Source: Radiation Research, 188(6) : 677-684

Published By: Radiation Research Society

URL: https://doi.org/10.1667/RR14693.1

RADIATION RESEARCH **188**, 677–684 (2017)
0033-7587/17 $15.00

DOI: 10.1667/RR14693.1

Measurement of DNA-Dependent Protein Kinase Phosphorylation Using Flow Cytometry Provides a Reliable Estimate of DNA Repair Capacity

Andris Abramenkovs[1] and Bo Stenerlöw

Department of Immunology, Genetics and Pathology, Rudbeck Laboratory, Uppsala University, SE-751 85 Uppsala, Sweden

Abramenkovs, A. and Stenerlöw, B. Measurement of DNA-Dependent Protein Kinase Phosphorylation Using Flow Cytometry Provides a Reliable Estimate of DNA Repair Capacity. *Radiat. Res.* 188, 677–684 (2017).

Uncontrolled generation of DNA double-strand breaks (DSBs) in cells is regarded as a highly toxic event that threatens cell survival. Radiation-induced DNA DSBs are commonly measured by pulsed-field gel electrophoresis, microscopic evaluation of accumulating DNA damage response proteins (e.g., 53BP1 or γ-H2AX) or flow cytometric analysis of γ-H2AX. The advantage of flow cytometric analysis is that DSB formation and repair can be studied in relationship to cell cycle phase or expression of other proteins. However, γ-H2AX is not able to monitor repair kinetics within the first 60 min postirradiation, a period when most DSBs undergo repair. A key protein in non-homologous end joining repair is the catalytic subunit of DNA-dependent protein kinase. Among several phosphorylation sites of DNA-dependent protein kinase, the threonine at position 2609 (T2609), which is phosphorylated by ataxia telangiectasia mutated (ATM) or DNA-dependent protein kinase catalytic subunit itself, activates the end processing of DSB. Using flow cytometry, we show here that phosphorylation at T2609 is faster in response to DSBs than γ-H2AX. Furthermore, flow cytometric analysis of T2609 resulted in a better representation of fast repair kinetics than analysis of γ-H2AX. In cells with reduced ligase IV activity, and wild-type cells where DNA-dependent protein kinase activity was inhibited, the reduced DSB repair capacity was observed by T2609 evaluation using flow cytometry. In conclusion, flow cytometric evaluation of DNA-dependent protein kinase T2609 can be used as a marker for early DSB repair and gives a better representation of early repair events than analysis of γ-H2AX.

INTRODUCTION

Most of the cellular toxicity induced by ionizing radiation stems from misrepaired or unrepaired DNA double-strand breaks (DSBs) (*1*). The ability to repair DSBs is vital for cell survival. Therefore, to repair these potentially lethal lesions, human cells have evolved two distinct repair pathways: non-homologous end joining (NHEJ) and homologous recombination (HR) (*2*). The choice between HR and NHEJ is regulated in a cell cycle-dependent manner, where HR is more active during S and G_2 phase, while NHEJ can participate in DSB repair during all stages of the cell cycle (*3*). Estimates of repair capacity in relationship to cell cycle phase, protein deficiencies and inhibitor treatments are vital for understanding DSB repair mechanisms.

Phosphorylated H2AX at S139 (γ-H2AX) is a commonly used marker of DSBs and can be detected using fluorescence microscopy (*4*) or flow cytometry (*5*). In response to DNA damage, H2AX can be phosphorylated by either ataxia telangiectasia mutated (ATM) or DNA-PKcs. The maximum intensity of γ-H2AX in cells is usually reached within 30–60 min postirradiation (*6, 7*) and it varies depending on cell cycle stage (*5*). However, the results from electrophoretic assays, such as pulsed-field gel electrophoresis (PFGE), show that repair-competent cells remove 60–70% of the initial DSBs within 1 h postirradiation (*8, 9*). Thus, the fast repair kinetics is lost when γ-H2AX is used as a DSB marker in flow cytometry. Although γ-H2AX is a widely-used marker of DSBs, it may also give a false-positive signal. For example, in hypoxic conditions γ-H2AX can be activated without the presence of DSBs (*10*).

Non-homologous end joining is the predominant repair pathway in cells and has been recently extensively reviewed (*11*). One of the key components in NHEJ is the catalytic subunit of DNA-dependent protein kinase (DNA-PKcs), which is a member of the PIKK family (*12*) and is phosphorylated at various sites upon induction of DSBs (*13*). During DSB repair, DNA-PKcs phosphorylates KU, Artemis, XRCC4 and ligase IV. Additionally, it can autophosphorylate itself at phosphorylation site S2056, which is positioned within the PQR cluster (*14*). Another important phosphorylation site in DNA-PKcs, T2609, is

Editor's note. The online version of this article (DOI: 10.1667/RR14693.1) contains supplementary information that is available to all authorized users.

[1] Address for correspondence: Department of Immunology, Genetics and Pathology, Rudbeck Laboratory, SE-751 85 Uppsala, Sweden; e-mail: Andris.Abramenkovs@igp.uu.se.

located at the ABCDE cluster, which is phosphorylated by ATM or DNA-PKcs itself (*15*). These two phosphorylation sites have distinct functions during DSB repair: phosphorylation of T2609 activates the end processing of DSBs (*14*), while the phosphorylation of the S2056 leads to ligation of DSBs (*16*). This indicates that T2609 could be used for evaluation of early repair events. Furthermore, foci of phosphorylated DNA-PKcs at T2609 co-localizes with γ-H2AX and 53BP1 foci in response to radiation exposure (*13, 17*).

In this study using flow cytometry, we show how pDNA-PKcs T2609 can serve as a marker for early DSB repair events and provide better representation of fast repair kinetics than previously reported analyses of γ-H2AX.

MATERIALS AND METHODS

Cells

GM5758, GM16088 and AG07217 cells were acquired from Coriell Institute (Camden, NJ) and were grown in Eagle's minimum essential medium (EMEM; Biochrom/Merck, Darmstadt, Germany). HCT116 and A431 cells were purchased from ATCC® (Gaithersburg, MD) and were grown in McCoy's 5A modified media and Ham's F-10 media, respectively. All media were supplemented with 9% fetal bovine serum (FBS; Sigma-Aldrich® LLC, St. Louis, MO), 100 IU/ml penicillin and streptomycin mix (Gibco®, Grand Island, NY) and 2 m*M* L-glutamine (Biochrom/Merck). Additionally, GM5758 and GM16088 were supplemented with 1× MEM vitamin solution (Gibco).

Flow Cytometry

Before irradiation, cells were cooled on ice for 20 min. Cells were then irradiated on ice to prevent the phosphorylation of proteins. For NU7441 (Selleckchem, Houston, TX) treatment, cells were pretreated for 1 h with 5 μ*M* NU7441 before irradiation. Gamma radiation was delivered at a dose rate of ~1 Gy/min using Gammacell® 40 (Gammacell extractor 40; MDS Nordion™ Inc., Ottawa, Canada). After 10 Gy photon irradiation, cold media was replaced with fresh pre-warmed media with or without NU7441. Cells were then trypsinized and placed in a pre-cooled centrifuge, which marked the end of repair. Cells were spun for 1 min at 200*g* and washed with ice cold 1× phosphate buffered saline (PBS) followed by another centrifugation for 1 min at 200*g*. After decanting the PBS, cells were carefully mixed with –20°C cold 70% ethanol. Samples were subsequently kept for at least 2 days at 4°C. Cells were then spun down and incubated in wash buffer (1% BSA and 0.1% Triton™ X-100 diluted in 1× PBS) for 30 min. Further 1:200 dilution of anti-DNA-PKcs T2609 (Abcam®, Cambridge, UK) and mouse monoclonal anti-γ-H2AX antibodies (JBW301 clones, cat. nos. 05-636 and 05-636-I; Merck) or rabbit monoclonal anti-γ-H2AX (EP854(2)Y clone, cat. no. ab81299; Abcam) were applied in wash buffer and incubated overnight at 4°C. On the following day, primary antibodies were discarded after centrifugation at 200*g* and cells were washed once in wash buffer. Afterwards, secondary antibodies conjugated with Alexa Fluor® 488 or APC (Abcam) were diluted in wash buffer (1:400 ratio) and incubated for 90 min at 4°C. Cells were washed once with wash buffer followed by incubation for 1 h with 1 μg/ml with DAPI (Thermo Fisher Scientific, Stockholm, Sweden) diluted in wash buffer. Cells were spun down and diluted in 1× PBS. At least 10,000 events were recorded using Cyflow® Cube 6 (Sysmex Partec, Gorlitz, Germany), BD LSR II and Fortessa™ (both from BD Biosciences, Franklin Lakes, NJ) or CytoFLEX (Beckman Coulter, Krefeld, Germany). To analyze H2AX and T2609 phosphorylation at different cell cycle stages, asynchronous cells were separated in G_1, S and G_2/M according to DAPI signal. Median fluorescence intensity of phosphorylated H2AX or DNA-PKcs was then determined in each subpopulation. Data were analyzed using FCS Express 4 (DeNovo Software, Los Angeles, CA) or FACSDiva™ software (BD Biosciences).

Pulsed-Field Gel Electrophoresis

Cells for PFGE were prelabeled for 2–6 doubling times with 2 kBq/ml of C-14 thymidine. Before irradiation, cells for $t = 0$ were trypsinized and embedded in InCert™ low-gelling-point agarose (Lonza, Morristown, NJ). Plugs, containing cells, were placed in ice-cold serum-free media while cells for other time points were placed on ice for 20 min. Irradiation with 40 Gy was performed on ice with dose rate of ~1 Gy per min. After irradiation, repair was started by replacing cold media with prewarmed fresh media. Cells were then trypsinized, embedded in low-gelling-point agarose and placed in 4°C, which was marked as the end of DSB repair. Agarose plugs containing cells were cooled for 20 min and then moved to lysis buffer composed of 1 mg/ml proteinase K and 2% sarkosyl diluted in 0.5 *M* EDTA (pH 8.0). The cells were lysed for at least 24 h at 4°C followed by complete removal of proteins with high-salt buffer (4 m*M* Tris; Sigma-Aldrich, Shanghai, China), 5 m*M* $MgCl_2$, 0.15 *M* KCl and 1.85 *M* NaCl, pH 7.5 (all from Merck) for 17–20 h. Before loading samples in 0.8% agarose gel (SeaKem® Gold; Lonza) the plugs were washed twice in 0.1 *M* EDTA and once in 0.5× TBE for 1 h per wash. The DNA was separated in 0.5× TBE using the following pulses: 10 min pulses for 3 h; 20 min pulses for 5 h and 20 min; 30 min pulses for 8 h; 40 min pulses for 9 h and 20 min; and 60 min pulses for 20 h. The gel was then stained with ethidium bromide (0.5 μg/ml) for at least 4 h and destained in deionized water overnight. Further, DNA fragments larger and smaller than 5.7 Mbp were separated using *S. pombe* chromosomes (Bio-Rad® Laboratories Inc., Hercules, CA) as markers. The gel fragments then were loaded in plastic liquid scintillation vials. Deionized water (2 ml) was added to the smallest fragment, followed by adding 0.2 *M* HCl to all samples. Samples were then heated at 95°C for 1 h. After the samples were cooled, 5 ml of Quicksafe A liquid scintillation fluid (Zinsser Analytic, Bracknell, UK) was added. On the following day, signals from each sample were collected over 10 min (Wallac 1414 Win Spectral Liquid Scintillation Counter; PerkinElmer® Inc., Waltham, MA) in CPM mode. During analysis, background and control values were subtracted from all time points and ratio of fragments smaller than 5.7 Mbp to fragments larger than 5.7 Mbp were calculated. Starting values were then normalized to $t = 0$, expressed as percentage.

Foci Scoring

GM5758 and GM16088 cells were plated in chamber slides and 2 Gy irradiated at room temperature. Cells were washed in 1× PBS and fixated using 99% methanol for at least one day. Afterwards, cells were dipped in ice-cold acetone for 15 s and air dried. Blocking was performed for 1 h in 10% FBS-PBS followed by incubation overnight with primary anti-53BP1 (Abcam), anti-γ-H2AX or anti-pDNA-PKcs T2609 antibodies in concentrations of 1:1,000, 1:100 and 1:100 diluted in 1% FBS. On the following day, cells were washed 3 times in 1× PBS for 5 min and secondary antibodies Alexa Fluor 488 and 647 were applied for 1 h in 1% FBS-PBS in a concentration of 1:400. Furthermore, unbound secondary antibodies were removed by washing slides 3 times in 1× PBS for 5 min. Cell nuclei were stained with 1 μg/ml DAPI for 5 min, and glass slides were then washed in MQ water for 10 min and left to air dry. Afterwards, Vectashield® mounting media (Burlingame, CA) was applied and glass slides were covered with a coverslip and sealed with nail polish. Finally, images were captured using the Zeiss LSM 700 (Jena, Germany) confocal microscope and analyzed using ImageJ plugin FociPicker3D (NIH, Bethesda, MD).

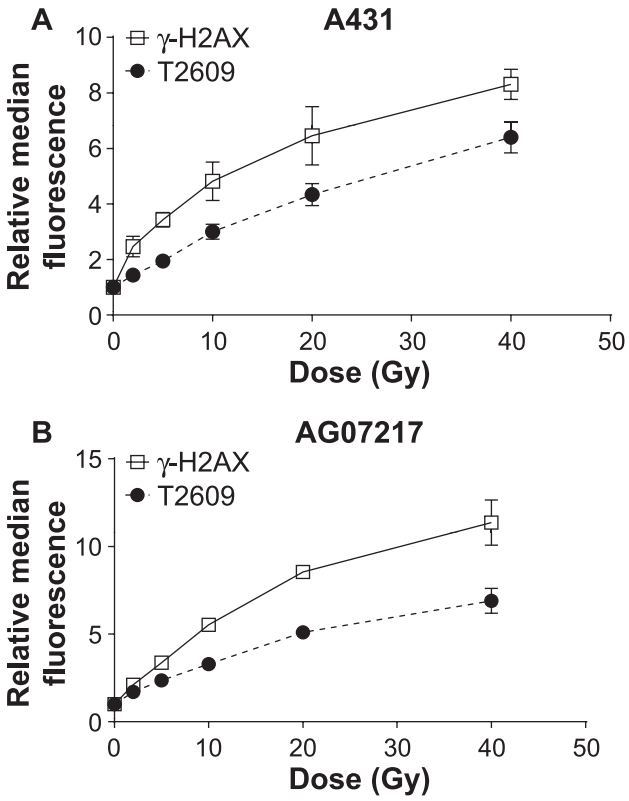

FIG. 1. Dose response of DNA-PKcs T2609 and γ-H2AX phosphorylation 30 min postirradiation in asynchronous populations of A431 (panel A) and AG07217 (panel B) cells after increasing gamma radiation doses. Data are shown from two independent experiments for γ-H2AX (JBW301 clone) and from 4–7 independent experiments for DNA-PKcs T2609. The error bars represent SEM.

Statistical Analysis

It was assumed that in all experiments data were normally distributed and comparison among groups was made using unpaired *t* test, and all tests results with $P < 0.05$ were considered statistically significant. Multiple comparisons were made with one-way analysis of variance (ANOVA) using Bonferroni correction. All tests were performed in GraphPad Prism software, version 6.07 (LaJolla, CA).

RESULTS

To investigate whether pDNA-PKcs can be used to score DSB repair using flow cytometry, A431 and AG07217 cells were irradiated with increasing dose and left to repair for 30 min (Fig. 1A and B). The pDNA-PKcs T2609 displayed increasing median fluorescence intensity with increasing dose. The scoring of pDNA-PKcs S2056 was more challenging due to significantly lower signal ratios (data not shown). Furthermore, dose-response analysis in these cell lines revealed that pDNA-PKcs signal was significantly lower than γ-H2AX signal in irradiated A431 cells (doses between 2–40 Gy; $P < 0.05$) and AG07217 cells (doses between 10–40 Gy; $P < 0.05$). To determine if it was possible to score pDNA-PKcs T2609 and γ-H2AX simultaneously, a rabbit monoclonal antibody anti-γ-H2AX was tested and data are shown in Supplementary Fig. S1 (http://dx.doi.org/10.1667/RR14693.1.S1). It was observed that rabbit monoclonal antibody clone EP854(2)Y displayed lower phosphorylation levels than mouse monoclonal antibody clone JBW301. Therefore, for the kinetic studies, the JBW301 clone was selected. In both cell lines, the 10 Gy dose showed approximately three times higher median fluorescence intensity of pDNA-PKcs T2609 than

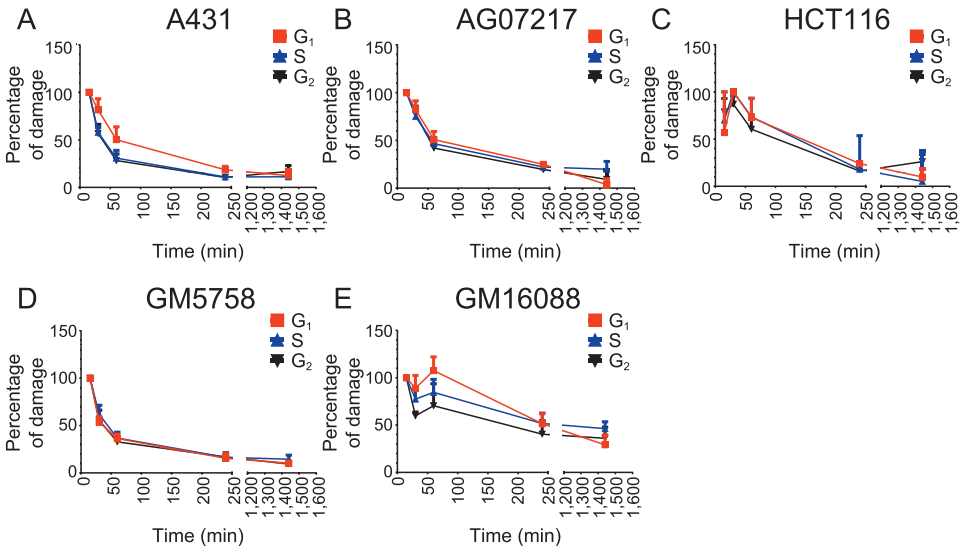

FIG. 2. pDNA-PKcs T2609 displays similar repair kinetics in all cell cycle phases. Panels A–E: A431, AG07217, HCT116, GM5758 and GM16088 cells, respectively, were 10 Gy gamma irradiated, trypsinized, fixed and stained for cell cycle and pDNA-PKcs T2609. Median fluorescence intensity changes in G_1 (red), S (blue) and G_2 (black) phases are shown. Median fluorescence intensity was normalized to 15 min repair time with respect to each cell cycle phase. Results from 3–8 experiments are shown as the mean and error bars represents SEM.

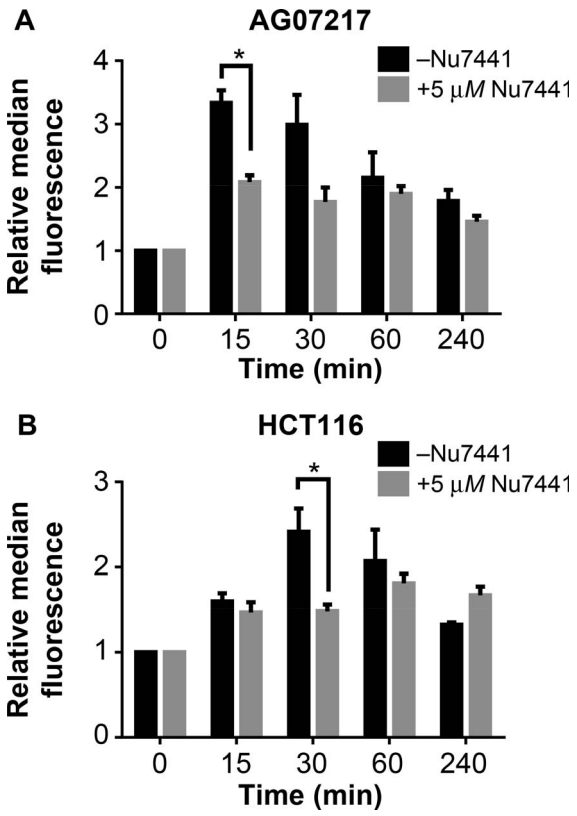

FIG. 3. NU7441 delays phosphorylation and dephosphorylation of DNA-PKcs T2609 in AG07217 (panel A) and HCT116 cells (panel B). AG071217 and HCT116 cells were treated without (black bars) or with (gray bars) 5 μ*M* NU7441 for 1 h before irradiation. After irradiation, fresh media with or without drug was applied. Relative median fluorescence intensity change of pDNA-PKcs T2609 over 4 h was measured in asynchronous population. Data was normalized to nonirradiated cell median fluorescence intensity in each treatment group individually, and error bars represent SEM from 3–4 independent experiments. $*P < 0.05$.

controls, thus in the following experiments this dose was used.

It is known that H2AX phosphorylation depends on DNA content and is not equal in all cell cycle stages (*5*), therefore the pDNA-PKcs T2609 over cell cycle was scored (Supplementary Fig. S2; http://dx.doi.org/10.1667/RR14693.1.S1). It was observed that the phosphorylation of DNA-PKcs T2609 increases with cell progression into S and G_2 phase (Supplementary Fig. 2A and B) in control and irradiated cells. However, upon irradiation the median fluorescence intensity increases, while the ratio of phosphorylation does not change drastically between G_1, S and G_2 (Supplementary Fig. 2C). Since high doses of radiation effect cell cycle distribution several hours after exposure, phosphorylation of each cell cycle stage should be evaluated separately. Therefore, the median fluorescence intensity of the whole population can be used only during a period when no significant changes in cell cycle are observed.

In further experiments, five different cell lines were 10 Gy irradiated and retention of pDNA-PKcs T2609 was measured in all cell cycle stages (Fig. 2A–E). All cell lines were proficient in DSB repair and displayed normal repair kinetics, except GM16088, which are ligase IV-hypomorphic cells and have 5–10% of wild-type ligase activity (*18*). Surprisingly, all cells showed similar repair kinetics in G_1, S and G_2 when normalized to their respective cell cycle stage. DNA-PKcs was rapidly phosphorylated after irradiation, with maximal phosphorylation observed 15–30 min postirradiation. Wild-type cells showed reduction of pDNA-PKcs T2609 within 60 min postirradiation while ligase IV hypomorphic cells displayed no changes in pDNA-PKcs T2609 median fluorescence intensity. At 4 h postirradiation, 9–26% of the initial ($t = 15$ min) pDNA-PKcs was present in wild-type cells, while 51% of pDNA-PKcs T2609 was still present in ligase IV-deficient GM16088 cells. Additionally, phosphorylation and dephosphorylation of γ-H2AX in irradiated A431 and AG07217 cells were compared with pDNA-PKcs T2609 (Supplementary Fig. 3A and B; http://dx.doi.org/10.1667/RR14693.1.S1), and both cell lines displayed faster phosphorylation and dephosphorylation of DNA-PKcs T2609 than γ-H2AX. It is important to note that the signal-to-noise ratio at 30 min postirradiation decreased in DNA-PKcs T2609, while γ-H2AX signal increased or remained stable, therefore, they affect the relative fluorescence intensity ratios differently (Fig. 1). This suggests that pDNA-PKcs T2609 better represents early DSB repair events than that of γ-H2AX that has been previously reported.

Furthermore, we investigated whether specific DNA-PKcs inhibitor NU7441 can induce detectable changes in DNA-PKcs phosphorylation status. It has previously been shown that NU7741 inhibits formation of S2056 foci (*19*), while the inhibitor treatment does not affect formation of T2609 foci or significantly affect ATM or ATR activity (*20*). AG07217 and HCT116 cells were treated with 5 μ*M* NU7441 for 1 h, irradiated, fixated and stained, and cells in asynchronous population were then analyzed (Fig. 3A and B). In both cell lines, NU7441 delayed phosphorylation of DNA-PKcs T2609, in AG07217 at 15 min postirradiation ($P < 0.002$) and in HCT116 cells at 30 min ($P < 0.04$). Intriguingly, after NU7441 treatment, pDNA-PKcs did not reach same levels as in nontreated samples, and there was no significant reduction of median fluorescence intensity changes over a 4 h period in either cell line ($P > 0.05$), indicating inhibited DSB repair.

Pulsed-field gel electrophoresis is one of the most precise methods to measure the kinetics of DSB rejoining. Thus, repair of all five cell lines was measured using PFGE and compared with dephosphorylation of DNA-PKcs T2609 (Fig. 4A–E). Both methods showed comparable trends in repair kinetics in all cell lines as early as 30 min postirradiation. However, HCT116 cells displayed delayed phosphorylation and dephosphorylation of pDNA-PKcs T2609, while no repair delay was observed in PFGE (Fig. 4C).

Since flow cytometric evaluation showed significant reduction of pDNA-PKcs in wild-type (GM5758) cells

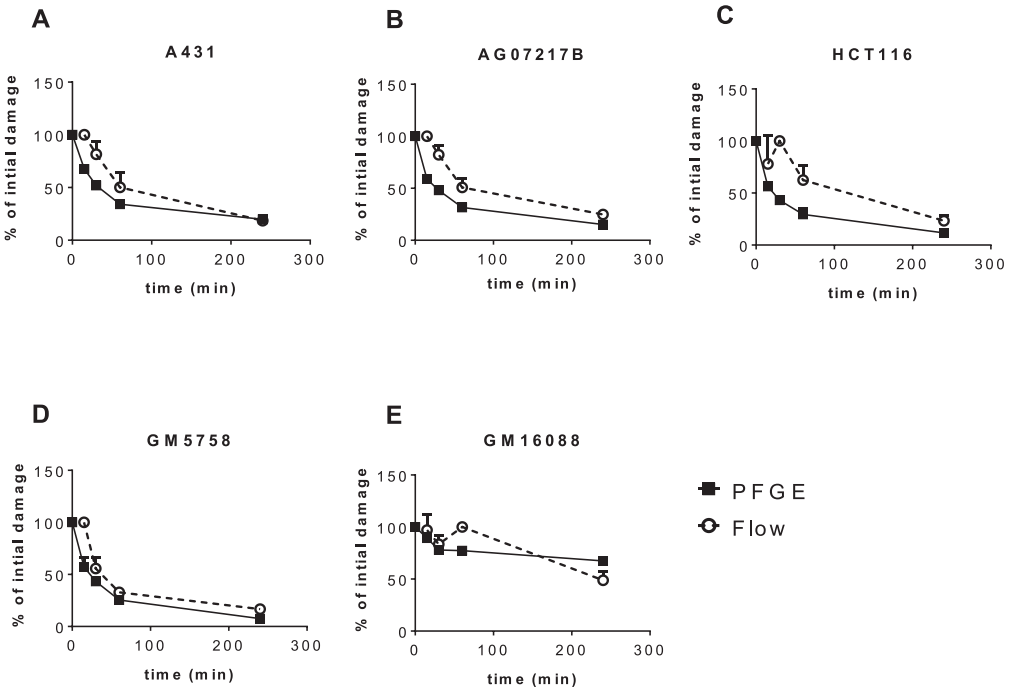

FIG. 4. pDNA-PKcs T2609 intensity changes in G_1 (black dotted) represents similar repair kinetics as PFGE (black solid) in (panels A–E): A431, AG07217, HCT116, GM5758 and GM16088 cells, respectively. Controls were subtracted and data normalized to the maximum signal in each assay separately. Data from 3–8 experiments are shown, and error bars represent SEM. Dotted lines represent the G_1 data set transferred from Fig. 2.

compared to ligase IV hypomorphic (GM16088) cells at 1 and 4 h postirradiation ($P = 0.0069$ and 0.0385), we compared these flow cytometric results with foci scoring assay. Ligase IV hypomorphic cells (GM16088) and wild-type fibroblasts GM5758 were irradiated and stained with 53BP1, γ-H2AX and pDNA-PKcs T2609. The foci count increased within 1 h in both cell lines for all of the markers analyzed (Fig. 5A–C). Similarly, as in PFGE and flow cytometric analysis of pDNA-PKcs T2609, ligase IV hypomorphic cells displayed an increased number of foci for DNA-PKcs T2609, 53BP1and γ-H2AX 4 h postirradiation compared to wild-type cells ($P = 0.0045$; $P = 0.0064$; $P = 0.0136$).

The removal of pDNA-PKcs T2609, 53BP1 and γ-H2AX foci displayed similar kinetics, albeit it was slower in ligase IV hypomorphic cells. In wild-type cells, the changes of pDNA-PKcs at T2609 observed with flow cytometry represented faster DSB repair kinetics than foci scoring assay (Fig. 6) as early as 1 h postirradiation ($P < 0.001$), while both assays resulted in similar kinetics in ligase IV hypomorphic cells.

DISCUSSION

DNA-PKcs plays an important role in DSB repair and signaling. It not only directly participates in DSB repair, but also activates and recruits other repair proteins to the DSB sites, thus making it a good candidate for analysis of DSB repair kinetics. In this study, we show that DNA-PKcs phosphorylation at T2609, measured with flow cytometry, can be used to score early DSB repair events in radiation-induced DSBs. Similar to γ-H2AX, DNA-PKcs phosphorylation at T2609 is dependent on DNA content in cells. Thus, cell cycle stage should be taken in account when changes in fluorescence intensity are assessed, which is especially important after longer repair times when cells become arrested in the G_2/M phase. However, when pDNA-PKcs T2609 signal was normalized according to the specific cell cycle stage, the fluorescence intensity increased and decayed similarly in all cell cycle phases. This suggests that NHEJ proteins might have an important role in DNA repair in S phase as well, although in this phase HR is the preferred repair pathway. Recently, it has been shown that BRCA1 interferes with phosphorylation of DNA-PKcs at S2056 in the S phase, while phosphorylation of DNA-PKcs at T2609 is unaffected (*21*), which is consistent with the notion that pDNA-PKcs T2609 activates end processing (*14*). However, the exact involvement of DNA-PKcs functions in S phase repair still remains unclear; therefore, we recommend scoring pDNA-PKcs T2609 in the G_1 phase when evaluating DSB repair.

Cells defective in proteins involved in NHEJ display reduced DSB repair capacity and are radiosensitive. The ability to discriminate between wild-type and ligase IV hypomorphic cells can be useful in the characterization of SCID patients and in the selection of appropriate cancer

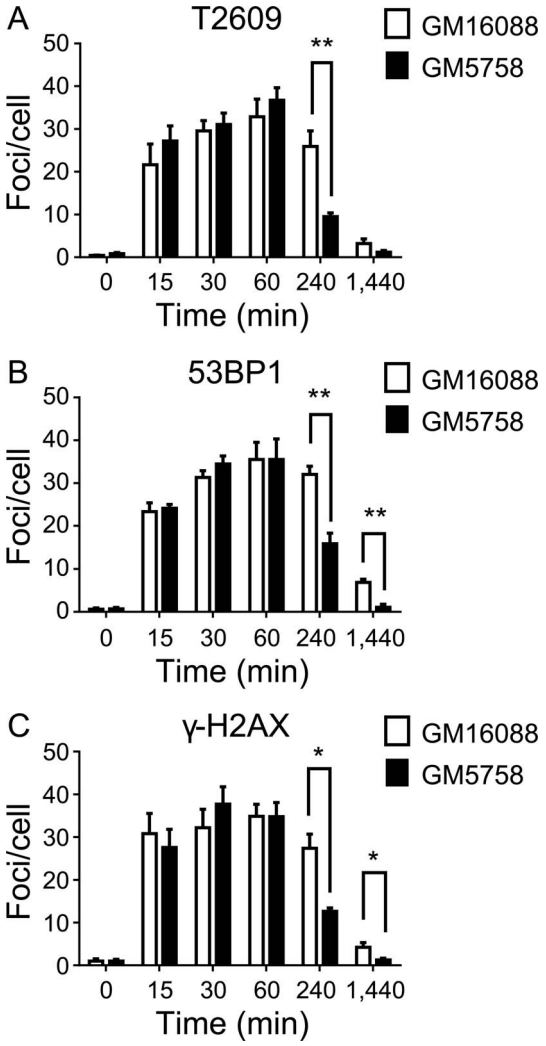

FIG. 5. Ligase IV hypomorphic cells remove foci slower than wild-type cells. Ligase IV hypomorphic cells GM16008 and wild-type cells GM5758 were 2 Gy irradiated and left to repair for the indicated time, fixated and stained for pDNA-PKcs T2609 (panel A), 53BP1 (panel B) and γ-H2AX (panel C). Mean values of the total foci count are represented from 3–4 independent experiments, and error bars represent SEM. At least one field of view was acquired from each experiment, and more than 50 cell nuclei were analyzed.

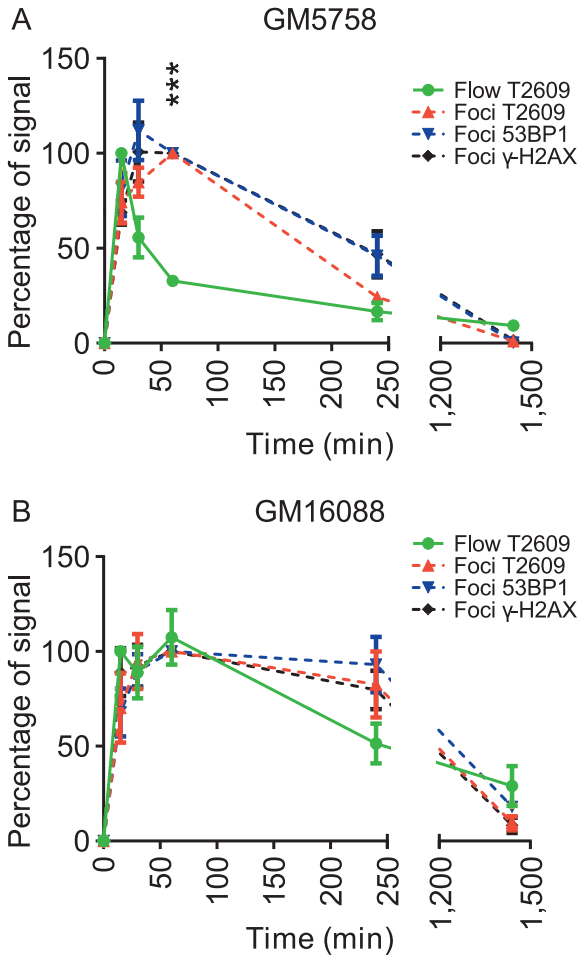

FIG. 6. Flow cytometric analysis of pDNA-PKcs represents better repair kinetics in wild-type cells than foci scoring assay. Kinetics of pDNA-PKcs T2609 in GM5758 (panel A) and ligase IV hypomorphic cells GM16088 (panel B) was compared using flow cytometry (green) and foci scoring (red). Additionally, 53BP1 and γ-H2AX foci kinetics is shown (blue and black). Data represents 3–4 independent experiments, and error bars display SEM. Dotted lines are transferred from Fig. 5 and solid lines represent repair in G_1 phase and have been transferred from Fig. 2. ***$P < 0.001$.

therapies. We and others have previously shown that treatment with NU7441 does not prevent formation of pDNA-PKcs foci (*19, 22, 23*). Therefore, in this study we used NU7441 to delay the phosphorylation of DNA-PKcs, which was successfully measured using flow cytometry. Intriguingly, the inhibitor treatment prevented DNA-PKcs phosphorylation and dephosphorylation over a 4 h time period in both cell lines. Thus, we suggest that pDNA-PKcs T2609 measurements using flow cytometry can potentially be used in DNA repair inhibitor screening and characterization. Taken together, these results provide evidence that pDNA-PKcs T2609 scoring with flow cytometry can be used to detect NHEJ defects in cells.

Interestingly, it was observed that HCT116 shows normal rejoining of DSBs as measured by PFGE, while flow cytometric analysis revealed delayed phosphorylation of DNA-PKcs T2609. It is known that HCT116 produces a truncated form of Mre11, which is part of MRN complex (*24*). The MRN complex is not only involved in processing of DSBs, but is also one of the first proteins involved in DSB signaling (*25*). Since there was no detectable DSB repair delay in PFGE, we speculate that the mutation in *MRE11* has a more prominent effect on signaling than actual repair of DSBs. Alternatively, it is possible that dephosphorylation of DNA-PKcs could be delayed due to a decreased amount of protein phosphatase 5 in cells (*26*).

In wild-type cells the foci assay exhibited slower kinetics than PFGE and flow cytometric assay. One explanation for this could be that during repair, foci decrease in size and fluorescence intensity, yet due to high sensitivity of

confocal microscopy, these sites are still detected as foci. It is possible to improve analysis of the kinetics in foci scoring assays by introducing size, volume or intensity thresholds; however, that would require more advanced analytic systems and extensive validation, and would reduce the processing speed. In this study, the foci scoring assay resulted in similar conclusions as PFGE and flow cytometry where ligase IV hypomorphic cells exhibits hindered repair. The main advantage of the foci scoring assay is the ability to score a low amount of damage induced in cells, and subnuclear localization and co-localization with other proteins. However, the analysis of pDNA-PKcs T2609 with flow cytometry provides better statistics, represents better repair kinetics and is less laborious. From all of these assays, the PFGE continues to provide more accurate estimates of DSB repair kinetics. Scoring DSB repair using pDNA-PKcs T2609 is not possible at early time points due to the delay of DNA-PKcs T2609 phosphorylation and in ATM-deficient cells, where T2609 phosphorylation is abolished (*15*). In contrast, there are no such limitations for PFGE, which measures physical rejoining of DSBs. The advantages of using flow cytometry over PFGE to score DSB repair are the ability to estimate repair in different populations and quantify repair in each cell cycle phase, as well as high throughput.

It is well established that γ-H2AX signal reaches maximum intensity approximately 30–60 min postirradiation (*6, 7*), while the electrophoretic assays show great reduction in DSBs at this period of time. In our study, pDNA-PKcs T2609 shows faster increase and decrease of maximum intensity, which can be explained by the fact that γ-H2AX is downstream of DNA-PKcs and is phosphorylated more extensively, which is further supported by the fact that the phosphorylation of γ-H2AX can reach up to megabases away from DSBs, while DNA-PKcs is usually localized to ~5 kbp around DSBs (*27*). Even though DNA-PKcs T2609 phosphorylation levels are lower than their respective γ-H2AX levels, the flow cytometric evaluation of pDNA-PKcs T2609 could still be useful in clinical settings where higher doses are used, e.g., during stereotactic ablative radiotherapy (*28*).

Additionally, we have observed that the ratio of pDNA-PKcs T2609 in nonirradiated and irradiated cells varies from cell line to cell line (data not shown). It is known that that DNA-PKcs T2609 phosphorylation occurs in mitosis where this marker co-localizes with mitotic spindle (*29*). Furthermore, the DNA-PKcs T2609 can be hyperphosphorylated in cancer cells driving the metastatic process (*30*). Taken together, these factors could explain the different noise-to-signal ratios found in different cells that cause the comparison of absolute pDNA-PKcs T2609 levels between different cell lines to be challenging. However, this does not affect analysis when relative phosphorylation level changes are measured, as the pDNA-PKcs T2609 increase is measured in irradiated cells and normalized to the respective controls.

In principle, it is possible to score γ-H2AX and pDNA-PKcs T2609 simultaneously. However, in this study the rabbit antibody EP854(2)Y did not provide results that were as robust as the widely-used mouse monoclonal antibody JBW301. With further optimization of antibodies and fixation protocols, it might be possible to score γ-H2AX and pDNA-PKcs T2609 in the same sample.

SUPPLEMENTARY INFORMATION

Fig. S1. Dose response of mouse monoclonal (JBW301) and rabbit monoclonal (EP854(2)Y) γ-H2AX antibodies in A431 and AG07217 cells. Solid line represents data transferred from Fig. 1. Data from 2–3 experiments are shown and error bars represent SEM.

Fig. S2. Radiation induces increase of DNA-PKcs T2609 phosphorylation. AG07217 cells were 10 Gy irradiated and left to repair for 30 min. Panel A: Bivariate analysis of DNA content and pDNA-PKcs results in increased phosphorylation in S and G_2 phases compared to G_1 phase in irradiated (red) and nonirradiated cells (blue). Irradiated cells in all cell cycle phases show increased phosphorylation of DNA-PKcs T2609 (panel B), while similar ratios are observed in control and irradiated cells when signal is normalized to G_1 (panel C).

Fig. S3. pDNA-PKcs T2609 represents more responsive repair kinetics than γ-H2AX. AG07217 (panel A) and A431 (panel B) cells were 10 Gy irradiated, left to repair, fixated and stained for pDNA-PKcs T2609 and γ-H2AX. Results are shown from 2–5 independent experiments for pDAN-PKcs and from a single experiment for H2AX. Whiskers represent SEM.

ACKNOWLEDGMENTS

This research was supported by grants from the Swedish Cancer Society and Swedish Radiation Safety Authority. Microscopic imaging and flow cytometry were performed with equipment maintained by the Science for Life Lab BioVis Platform, Uppsala University.

Received: November 28, 2016; accepted: August 10, 2017; published online: September 27, 2017

REFERENCES

1. Huang LC, Clarkin KC, Wahl GM. Sensitivity and selectivity of the DNA damage sensor responsible for activating p53-dependent G1 arrest. Proc Natl Acad Sci U S A 1996; 93:4827–32.
2. Mao Z, Bozzella M, Seluanov A, Gorbunova V. Comparison of nonhomologous end joining and homologous recombination in human cells. DNA Repair (Amst) 2008; 7:1765–71.
3. Karanam K, Kafri R, Loewer A, Lahav G. Quantitative live cell imaging reveals a gradual shift between DNA repair mechanisms and a maximal use of HR in mid S phase. Mol Cell 2012; 47:320–9.
4. Rogakou EP, Boon C, Redon C, Bonner WM. Megabase chromatin domains involved in DNA double-strand breaks in vivo. J Cell Biol 1999; 146:905–16.
5. MacPhail SH, Banath JP, Yu Y, Chu E, Olive PL. Cell cycle-dependent expression of phosphorylated histone H2AX: reduced

expression in unirradiated but not X-irradiated G1-phase cells. Radiat Res 2003; 159:759–67.

6. Tommasino F, Friedrich T, Jakob B, Meyer B, Durante M, Scholz M. Induction and processing of the radiation-induced gamma-H2AX signal and its link to the underlying pattern of DSB: a combined experimental and modelling study. PLoS One 2015; 10:e0129416.
7. Kinner A, Wu W, Staudt C, Iliakis G. Gamma-H2AX in recognition and signaling of DNA double-strand breaks in the context of chromatin. Nucleic Acids Res 2008; 36:5678–94.
8. Stenerlow B, Karlsson KH, Cooper B, Rydberg B. Measurement of prompt DNA double-strand breaks in mammalian cells without including heat-labile sites: results for cells deficient in nonhomologous end joining. Radiat Res 2003; 159:502–10.
9. Kinner A, Wu W, Staudt C, Iliakis G. Gamma-H2AX in recognition and signaling of DNA double-strand breaks in the context of chromatin. Nucleic Acids Res 2008; 36:5678–94.
10. Wrann S, Kaufmann MR, Wirthner R, Stiehl DP, Wenger RH. HIF mediated and DNA damage independent histone H2AX phosphorylation in chronic hypoxia. Biol Chem 2013; 394:519–28.
11. Yang K, Guo R, Xu D. Non-homologous end joining: advances and frontiers. Acta Biochim Biophys Sin (Shanghai) 2016; 48:632–40.
12. Hartley KO, Gell D, Smith GC, Zhang H, Divecha N, Connelly MA, et al. DNA-dependent protein kinase catalytic subunit: a relative of phosphatidylinositol 3-kinase and the ataxia telangiectasia gene product. Cell 1995; 82:849–56.
13. Chan DW, Chen BP, Prithivirajsingh S, Kurimasa A, Story MD, Qin J, et al. Autophosphorylation of the DNA-dependent protein kinase catalytic subunit is required for rejoining of DNA double-strand breaks. Genes Dev 2002; 16:2333–8.
14. Meek K, Douglas P, Cui X, Ding Q, Lees-Miller SP. trans Autophosphorylation at DNA-dependent protein kinase's two major autophosphorylation site clusters facilitates end processing but not end joining. Mol Cell Biol 2007; 27:3881–90.
15. Chen BP, Uematsu N, Kobayashi J, Lerenthal Y, Krempler A, Yajima H, et al. Ataxia telangiectasia mutated (ATM) is essential for DNA-PKcs phosphorylations at the Thr-2609 cluster upon DNA double strand break. J Biol Chem 2007; 282:6582–7.
16. Cui X, Yu Y, Gupta S, Cho YM, Lees-Miller SP, Meek K. Autophosphorylation of DNA-dependent protein kinase regulates DNA end processing and may also alter double-strand break repair pathway choice. Mol Cell Biol 2005; 25:10842–52.
17. Wang J, He L, Fan D, Ding D, Wang X, Gao Y, et al. Establishment of a gamma-H2AX foci-based assay to determine biological dose of radon to red bone marrow in rats. Sci Rep 2016; 6:30018.
18. Girard PM, Kysela B, Harer CJ, Doherty AJ, Jeggo PA. Analysis of DNA ligase IV mutations found in LIG4 syndrome patients: the impact of two linked polymorphisms. Hum Mol Genet 2004; 13:2369–76.
19. Chatterjee P, Plesca D, Mazumder S, Boutros J, Yannone SM, Almasan A. Defective chromatin recruitment and retention of NHEJ core components in human tumor cells expressing a cyclin E fragment. Nucleic Acids Res 2013; 41:10157–69.
20. Leahy JJ, Golding BT, Griffin RJ, Hardcastle IR, Richardson C, Rigoreau L, et al. Identification of a highly potent and selective DNA-dependent protein kinase (DNA-PK) inhibitor (NU7441) by screening of chromenone libraries. Bioorg Med Chem Lett 2004; 14:6083–7.
21. Davis AJ, Chi L, So S, Lee KJ, Mori E, Fattah K, et al. BRCA1 modulates the autophosphorylation status of DNA-PKcs in S phase of the cell cycle. Nucleic Acids Res 2014; 42:11487–501.
22. Gustafsson AS, Abramenkovs A, Stenerlow B. Suppression of DNA-dependent protein kinase sensitize cells to radiation without affecting DSB repair. Mutat Res 2014; 769:1–10.
23. Javvadi P, Makino H, Das AK, Lin Y-F, Chen DJ, Chen BP, et al. Threonine 2609 phosphorylation of the DNA-dependent protein kinase is a critical prerequisite for epidermal growth factor receptor mediated radiation resistance. Mol Cancer Res 2012; 10:1359–68.
24. Wen Q, Scorah J, Phear G, Rodgers G, Rodgers S, Meuth M. A mutant allele of MRE11 found in mismatch repair-deficient tumor cells suppresses the cellular response to DNA replication fork stress in a dominant negative manner. Mol Biol Cell 2008; 19:1693–705.
25. Kijas AW, Lim YC, Bolderson E, Cerosaletti K, Gatei M, Jakob B, et al. ATM-dependent phosphorylation of MRE11 controls extent of resection during homology directed repair by signalling through exonuclease 1. Nucleic Acids Res 2015; 43:8352–67.
26. Wechsler T, Chen BP, Harper R, Morotomi-Yano K, Huang BC, Meek K, et al. DNA-PKcs function regulated specifically by protein phosphatase 5. Proc Natl Acad Sci U S A 2004; 101:1247–52.
27. Caron P, Choudjaye J, Clouaire T, Bugler B, Daburon V, Aguirrebengoa M, et al. Non-redundant Functions of ATM and DNA-PKcs in response to DNA double-strand breaks. Cell Rep 2015; 13:1598–609.
28. Simeonova AO, Fleckenstein K, Wertz H, Frauenfeld A, Boda-Heggemann J, Lohr F, et al. Are three doses of stereotactic ablative radiotherapy (SABR) more effective than 30 doses of conventional radiotherapy? Transl Lung Cancer Res 2012; 1:45–53.
29. Shang ZF, Huang B, Xu QZ, Zhang SM, Fan R, Liu XD, et al. Inactivation of DNA-dependent protein kinase leads to spindle disruption and mitotic catastrophe with attenuated checkpoint protein 2 phosphorylation in response to DNA damage. Cancer Res 2010; 70:3657–66.
30. Goodwin JF, Kothari V, Drake JM, Zhao S, Dylgjeri E, Dean JL, et al. DNA-PKcs-mediated transcriptional regulation drives prostate cancer progression and metastasis. Cancer Cell 2015; 28:97–113.